

Exclusive ρ^0 meson electroproduction from hydrogen at CLAS

C. Hadjidakis,^{1,2} M. Guidal,¹ M. Garçon,³ J.-M. Laget,³ E.S. Smith,⁴ M. Vanderhaeghen,^{4,5} G. Adams,³¹ P. Ambrozewicz,¹⁴ E. Anciant,³ M. Anghinolfi,¹⁹ B. Asavapibhop,²⁴ G. Asryan,⁴⁰ G. Audit,³ T. Auger,³ H. Avakian,^{4,2} H. Bagdasaryan,²⁸ J.P. Ball,⁶ S. Barrow,¹⁵ M. Battaglieri,¹⁹ K. Beard,²¹ M. Bektasoglu,^{27,28,39} M. Bellis,⁸ N. Benmouna,¹⁷ B.L. Berman,¹⁷ N. Bianchi,² A.S. Biselli,⁸ S. Boiarinov,^{4,20} B.E. Bonner,³³ S. Bouchigny,^{1,4} R. Bradford,⁸ D. Branford,¹³ W.J. Briscoe,¹⁷ W.K. Brooks,⁴ V.D. Burkert,⁴ C. Butuceanu,⁵ J.R. Calarco,²⁵ D.S. Carman,²⁷ B. Carnahan,⁹ C. Cetina,¹⁷ S. Chen,¹⁵ P.L. Cole,^{9,4} A. Coleman,⁵ D. Cords,⁴ P. Corvisiero,¹⁹ D. Crabb,³⁸ H. Crannell,⁹ J.P. Cummings,³¹ E. De Sanctis,² R. DeVita,¹⁹ P.V. Degtyarenko,⁴ L. Dennis,¹⁵ K.V. Dharmawardane,²⁸ K.S. Dhuga,¹⁷ J.-P. Didelez,¹ C. Djalali,³⁵ G.E. Dodge,²⁸ D. Doughty,^{10,4} P. Dragovitsch,¹⁵ M. Dugger,⁶ S. Dytman,³⁰ O.P. Dzyubak,³⁵ H. Egiyan,^{4,5} K.S. Egiyan,⁴⁰ L. Elouadrhiri,^{10,4} A. Empl,³¹ P. Eugenio,¹⁵ L. Farhi,³ R. Fatemi,³⁸ R.J. Feuerbach,⁴ T.A. Forest,²⁸ V. Frolov,³¹ H. Funsten,⁵ S.J. Gaff,¹² G. Gavalian,²⁸ G.P. Gilfoyle,³⁴ K.L. Giovanetti,²¹ P. Girard,³⁵ C.I.O. Gordon,¹⁸ R.W. Gothe,³⁵ K.A. Griffioen,⁵ M. Guillo,³⁵ M. Guler,²⁸ L. Guo,⁴ V. Gyurjyan,⁴ R.S. Hakobyan,⁹ J. Hardie,^{10,4} D. Heddle,^{10,4} F.W. Hersman,²⁵ K. Hicks,²⁷ H. Hleiqawi,²⁷ M. Holtrop,²⁵ E. Hourany,¹ J. Hu,³¹ C.E. Hyde-Wright,²⁸ Y. Ilieva,¹⁷ D. Ireland,¹⁸ M.M. Ito,⁴ D. Jenkins,³⁷ K. Joo,^{11,38} H.G. Juengst,¹⁷ J.H. Kelley,¹² J. Kellie,¹⁸ M. Khandaker,²⁶ K.Y. Kim,³⁰ K. Kim,²² W. Kim,²² A. Klein,²⁸ F.J. Klein,^{9,4} A.V. Klimenko,²⁸ M. Klusman,³¹ M. Kossov,²⁰ L.H. Kramer,^{14,4} S.E. Kuhn,²⁸ J. Kuhn,⁸ J. Lachniet,⁸ J. Langheinrich,³⁵ D. Lawrence,²⁴ T. Lee,²⁵ Ji Li,³¹ K. Livingstone,¹⁸ K. Lukashin,⁴ J.J. Manak,⁴ C. Marchand,³ L.C. Maximon,¹⁷ S. McAleer,¹⁵ J.W.C. McNabb,²⁹ B.A. Mecking,⁴ J.J. Melone,¹⁸ M.D. Mestayer,⁴ C.A. Meyer,⁸ K. Mikhailov,²⁰ R. Minehart,³⁸ M. Mirazita,² R. Miskimen,²⁴ L. Morand,³ S.A. Morrow,^{1,3} V. Muccifora,² J. Mueller,³⁰ G.S. Mutchler,³³ J. Napolitano,³¹ R. Nasseripour,¹⁴ S.O. Nelson,¹² S. Niccolai,^{1,17} G. Niculescu,^{21,27} I. Niculescu,^{21,17} B.B. Niczyporuk,⁴ R.A. Niyazov,^{4,28} M. Nozar,⁴ G.V. O'Rielly,¹⁷ M. Osipenko,¹⁹ K. Park,²² E. Pasyuk,⁶ G. Peterson,²⁴ S.A. Philips,¹⁷ N. Pivnyuk,²⁰ D. Pocanic,³⁸ O. Pogorelko,²⁰ E. Polli,² S. Pozdniakov,²⁰ B.M. Preedom,³⁵ J.W. Price,⁷ Y. Prok,³⁸ D. Protopopescu,¹⁸ L.M. Qin,²⁸ B.A. Raue,^{14,4} G. Riccardi,¹⁵ G. Ricco,¹⁹ M. Ripani,¹⁹ B.G. Ritchie,⁶ F. Ronchetti,^{2,32} P. Rossi,² G. Rosner,¹⁸ D. Rowntree,²³ P.D. Rubin,³⁴ F. Sabatié,^{3,28} K. Sabourov,¹² C. Salgado,²⁶ J.P. Santoro,^{37,4} V. Sapunenko,¹⁹ R.A. Schumacher,⁸ V.S. Serov,²⁰ A. Shafi,¹⁷ Y.G. Sharabian,^{4,40} J. Shaw,²⁴ S. Simionatto,¹⁷ A.V. Skabelin,²³ L.C. Smith,³⁸ D.I. Sober,⁹ M. Spraker,¹² A. Stavinsky,²⁰ S. Stepanyan,^{4,40} B.E. Stokes,¹⁵ P. Stoler,³¹ S. Strauch,¹⁷ M. Taiuti,¹⁹ S. Taylor,³³ D.J. Tedeschi,³⁵ U. Thoma,^{16,4} R. Thompson,³⁰ A. Tkabladze,²⁷ L. Todor,³⁴ C. Tur,³⁵ M. Ungaro,³¹ M.F. Vineyard,^{36,34} A.V. Vlassov,²⁰ K. Wang,³⁸ L.B. Weinstein,²⁸ H. Weller,¹² D.P. Weygand,⁴ C.S. Whisnant,^{21,35} M. Williams,⁸ E. Wolin,⁴ M.H. Wood,³⁵ A. Yegneswaran,⁴ J. Yun,²⁸ and L. Zana²⁵

(The CLAS Collaboration)

¹ *Institut de Physique Nucleaire ORSAY, Orsay, France*

² *INFN, Laboratori Nazionali di Frascati, Frascati, Italy*

³ *CEA-Saclay, Service de Physique Nucléaire, F91191 Gif-sur-Yvette, Cedex, France*

⁴ *Thomas Jefferson National Accelerator Facility, Newport News, Virginia 23606*

⁵ *College of William and Mary, Williamsburg, Virginia 23187-8795*

⁶ *Arizona State University, Tempe, Arizona 85287-1504*

⁷ *University of California at Los Angeles, Los Angeles, California 90095-1547*

⁸ *Carnegie Mellon University, Pittsburgh, Pennsylvania 15213*

⁹ *Catholic University of America, Washington, D.C. 20064*

¹⁰ *Christopher Newport University, Newport News, Virginia 23606*

¹¹ *University of Connecticut, Storrs, Connecticut 06269*

¹² *Duke University, Durham, North Carolina 27708-0305*

¹³ *Edinburgh University, Edinburgh EH9 3JZ, United Kingdom*

¹⁴ *Florida International University, Miami, Florida 33199*

¹⁵ *Florida State University, Tallahassee, Florida 32306*

¹⁶ *Physikalisches Institut der Universitaet Giessen, 35392 Giessen, Germany*

¹⁷ *The George Washington University, Washington, DC 20052*

¹⁸ *University of Glasgow, Glasgow G12 8QQ, United Kingdom*

¹⁹ *INFN, Sezione di Genova, 16146 Genova, Italy*

²⁰ *Institute of Theoretical and Experimental Physics, Moscow, 117259, Russia*

²¹ *James Madison University, Harrisonburg, Virginia 22807*

- ²² *Kyungpook National University, Daegu 702-701, South Korea*
²³ *Massachusetts Institute of Technology, Cambridge, Massachusetts 02139-4307*
²⁴ *University of Massachusetts, Amherst, Massachusetts 01003*
²⁵ *University of New Hampshire, Durham, New Hampshire 03824-3568*
²⁶ *Norfolk State University, Norfolk, Virginia 23504*
²⁷ *Ohio University, Athens, Ohio 45701*
²⁸ *Old Dominion University, Norfolk, Virginia 23529*
²⁹ *Penn State University, University Park, Pennsylvania 15260*
³⁰ *University of Pittsburgh, Pittsburgh, Pennsylvania 15260*
³¹ *Rensselaer Polytechnic Institute, Troy, New York 12180-3590*
³² *Universita' di ROMA III, 00146 Roma, Italy*
³³ *Rice University, Houston, Texas 77005-1892*
³⁴ *University of Richmond, Richmond, Virginia 23173*
³⁵ *University of South Carolina, Columbia, South Carolina 29208*
³⁶ *Union College, Schenectady, NY 12308*
³⁷ *Virginia Polytechnic Institute and State University, Blacksburg, Virginia 24061-0435*
³⁸ *University of Virginia, Charlottesville, Virginia 22901*
³⁹ *Sakarya University, Sakarya, Turkey*
⁴⁰ *Yerevan Physics Institute, 375036 Yerevan, Armenia*
(Dated: October 22, 2018)

The longitudinal and transverse components of the cross section for the $ep \rightarrow e'pp^0$ reaction were measured in Hall B at Jefferson Laboratory using the CLAS detector. The data were taken with a 4.247 GeV electron beam and were analyzed in a range of x_B from 0.2 to 0.6 and of Q^2 from 1.5 to 3.0 GeV². The data are compared to a Regge model based on effective hadronic degrees of freedom and to a calculation based on Generalized Parton Distributions. It is found that the transverse part of the cross section is well described by the former approach while the longitudinal part can be reproduced by the latter.

PACS numbers: 13.60.Fz, 12.38.Bx, 13.60.Le

Understanding the precise nature of the confinement of quarks and gluons inside hadrons has been an ongoing problem since the advent, about 30 years ago, of the theory that governs their interactions, quantum chromodynamics (QCD). In particular, the transition between the high energy (small distance) domain, where quarks are quasi-free, and the low energy (large distance) regime, where they form bound states and are confined in hadrons, is still not well understood.

The analysis of elementary processes, such as the exclusive electroproduction of a meson or a photon on the nucleon in the few GeV range, allows one to study this transition. In the case of exclusive meson electroproduction, the longitudinal and transverse polarizations of the (virtual) photon mediating the interaction provide two qualitatively different pieces of information about the nucleon structure.

Longitudinal photons, whose transverse size is inversely proportional to their virtuality, truly act as a microscope. At sufficiently large Q^2 , small distances are probed, and the asymptotic freedom of QCD justifies the understanding of the process in terms of partonic degrees of freedom and the use of perturbative QCD (pQCD) techniques. In particular, it has been recently shown [1, 2] that the non-perturbative information can be factorized in reactions such as exclusive vector meson electroproduction. Here the process can be described in terms of perturbative quark or gluon

exchanges whose momentum, flavor, and spin distributions inside the nucleon are parametrized in terms of the recently introduced Generalized Parton Distributions (GPD's) [3, 4, 5]. This is the so-called “handbag” diagram mechanism which is depicted in Fig. 1 (right diagram). At higher γ^*p center-of-mass energies, W , than considered in this letter, 2-gluon exchange processes also intervene [2, 6]. At low virtuality, Q^2 , of the photon, hadronic degrees of freedom are more relevant and, above the nucleon resonance region, the process is adequately described in terms of meson exchanges (Fig. 1, left diagram).

For transverse photons, however, this description in terms of quarks and gluons is not valid. A factorization into a hard and soft part does not hold [1, 2] and even at large Q^2 , there is no dominance of a “handbag” mechanism as in Fig. 1. “Soft” (non-perturbative) and “hard” (perturbative) physics compete over a wider range of Q^2 , and in practice it is necessary to take into account non-perturbative effects using hadron degrees of freedom. In order to access the fundamental partonic information when studying meson electroproduction processes, it is therefore highly desirable to isolate the longitudinal part of the cross section, which lends itself, at least at sufficiently high Q^2 , to pQCD techniques and interpretation. In this approach, however, several questions remain to be answered. What is the lowest Q^2 where a perturbative treatment is valid? What corrections need to be applied

to extend its validity to lower Q^2 ?

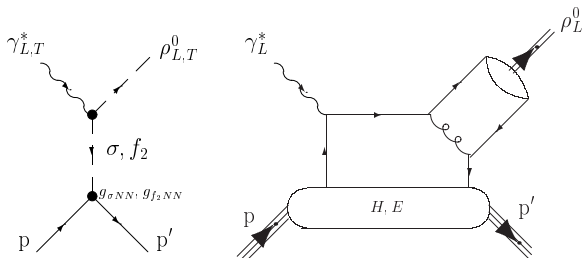


FIG. 1: The mechanisms for ρ^0 electroproduction at intermediate energies: at low Q^2 (left diagram) through the exchange of mesons, and at high Q^2 (right diagram) through the quark exchange “handbag” mechanism (valid for longitudinal photons) where H and E are the unpolarized GPD’s.

The aim of this letter is to address these questions using the recent measurement of the longitudinal and transverse cross sections of the $ep \rightarrow e'p\rho^0$ reaction, carried out at Jefferson Laboratory using the CEBAF Large Acceptance Spectrometer (CLAS) [7] in Hall B. This elementary process is one of the exclusive reactions on the nucleon which has the highest cross section, and for which the extraction of the longitudinal and transverse parts of the cross section can be accomplished using the ρ^0 decay angular distribution. On the theoretical side, formalisms and numerical estimates for both hadronic and partonic descriptions of the reaction have been developed, which can be compared to the transverse and longitudinal components of the cross section, respectively.

In the following, we will present the analysis results of the $ep \rightarrow e'p\rho^0$ reaction. Data were taken with an electron beam energy of 4.247 GeV impinging on an unpolarized liquid-hydrogen target. The integrated luminosity of this data set was about 1.5 fb^{-1} . The kinematic domain of the selected sample corresponds to Q^2 from 1.5 GeV² to 3.0 GeV². We analyzed data for W greater than 1.75 GeV, which corresponds to a range of x_B from 0.21 to 0.62. Our final data sample included about 2×10^4 $e'p\pi^+\pi^-$ events.

The ρ^0 meson decay to $\pi^+\pi^-$ was used to identify the reaction of interest. We identified the $ep \rightarrow e'p\pi^+\pi^-$ reaction using the missing mass technique by detecting the scattered electron, the recoil proton, and the positive pion. The electron was identified as a negative track with reconstructed energy deposition in the calorimeter which was consistent with the momenta determined from magnetic analysis, in combination with a signal in the Cerenkov counter. The proton and pion were identified as positive tracks, whose combination of flight times and momenta corresponded to their mass. Figure 2 (left plot) shows a typical missing mass distribution for $ep \rightarrow e'p\pi^+X$ events. Events were selected by the missing mass cut $-0.03 < M_X^2 < 0.06 \text{ GeV}^2$, consistent with

a missing π^- . Fig. 2 (center) shows the resulting $\pi^+\pi^-$ invariant mass spectrum. The ρ^0 peak is clearly visible, sitting on a large non-resonant $\pi^+\pi^-$ background.

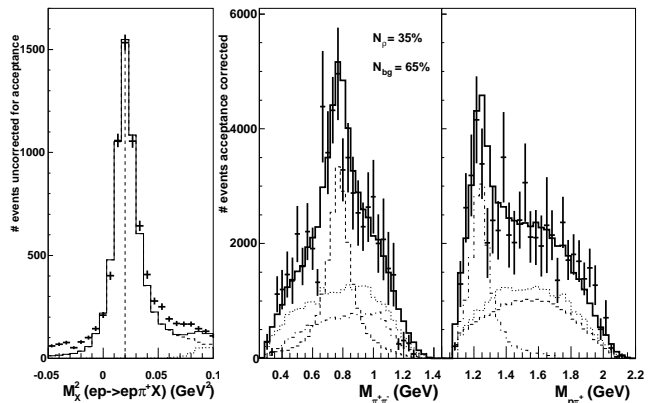


FIG. 2: Left plot: an example of a squared missing mass $M_X^2(ep \rightarrow e'p\pi^+X)$ spectrum (for a scattered electron momentum between 1.9 and 2.2 GeV). Points with error bars show the experimental data and the solid lines represent the results of simulations for the channels $e'p\pi^+\pi^-$ (dashed line), $e'p\pi^+\pi^-\pi^0$ (dotted line) and the sum of the two (solid line). The vertical dashed line is located at the missing mass squared of a pion. Central and right plots: an example of the $\pi^+\pi^-$ and $p\pi^+$ invariant masses, respectively (for the interval $1.63 < Q^2 < 1.76 \text{ GeV}^2$ and $0.28 < x_B < 0.35$). Points with error bars show the experimental data and the lines correspond to the results of fits for the channels $ep \rightarrow e'p\rho^0$ (dashed line), $ep \rightarrow e'\Delta^{++}\pi^-$ (dash-dotted line), non-resonant $ep \rightarrow e'p\pi^+\pi^-$ (dotted line) and the sum of the three processes (solid line).

The unpolarized $ep \rightarrow e'p\pi^+\pi^-$ reaction is fully defined by seven independent kinematical variables which we have chosen as: Q^2 and x_B , which define the virtual photon kinematics; t , the invariant squared momentum transfer between the virtual photon and the final pion pair (*i.e.* the ρ^0 meson when this particle is produced); $M_{\pi^+\pi^-}$, the invariant mass of the $\pi^+\pi^-$ system; θ_{hel} and ϕ_{hel} , the π^+ decay angles in the $\pi^+\pi^-$ rest frame; and Φ , the azimuthal angle between the hadronic and leptonic planes. The CLAS acceptance and efficiency were calculated for each of these 7-dimensional bins using a GEANT-based simulation of several hundred million events. The event distributions were generated according to Ref. [8], which includes the three main contributions above the resonance region to the $e'p\pi^+\pi^-$ final state: diffractive $ep \rightarrow e'p\rho^0$, t -channel $ep \rightarrow e'\Delta^{++}\pi^-$, and non-resonant (phase space) $ep \rightarrow e'p\pi^+\pi^-$. Each of these contributions to the event generator was matched to the world’s data on differential and total cross sections, and then extrapolated to our kinematical domain. We were then able to extract a total cross section for the $ep \rightarrow e'p\pi^+\pi^-$ channel in good agreement with world’s

data where the kinematics overlapped. The event generator also includes radiative effects following the Mo and Tsai prescription [9] so that radiative corrections could be applied in each (Q^2, x_B) bin.

The main difficulty in determining the ρ^0 yield stems from its large width ($\Gamma_{\rho^0} \sim 150$ MeV), which does not allow for a unique determination of the separate contributions due to the resonant ρ^0 production and non-resonant $\pi^+\pi^-$ pairs. We simultaneously fitted the two 3-fold differential cross sections $d^3\sigma/dQ^2 dx_B dM_{\pi^+\pi^-}$ and $d^3\sigma/dQ^2 dx_B dM_{p\pi^+}$ to determine the weight of the three channels mentioned earlier, leading to the $e'p\pi^+\pi^-$ final state (see Fig. 2, central and right plots). The mass spectra of the ρ^0 and Δ^{++} are generated according to standard Breit-Wigner distributions and the non-resonant $p\pi^+\pi^-$ final state according to phase space. This background estimation procedure, along with the CLAS acceptance modeling, is one of the dominant sources of systematic uncertainty which, in total, ranges from 10% to 25%. More sophisticated shapes for the ρ^0 mass spectra were also investigated but led to consistent numbers of ρ^0 's within these error bars.

The final step of the analysis consisted in separating the longitudinal and the transverse parts of the $ep \rightarrow e'p\rho^0$ cross section. The determination of these two contributions was accomplished under the assumption of s -channel helicity conservation (SCHC) [10]. This hypothesis states, in simple terms, that the helicity of the virtual photon is directly transferred to the vector meson. The SCHC hypothesis originates from the vector meson dominance model which identifies vector meson electromagnetic production as an elastic process without spin transfer.

The validity of the SCHC hypothesis, which is only applicable at small momentum transfer t , can be tested experimentally through the analysis of the azimuthal angular distribution. We found that the r_{1-1}^{04} ρ^0 decay matrix element [11], which can be extracted from the ϕ_{hel} dependence, was compatible with zero at the 1.7 sigma level. We also found that the σ_{TT} and σ_{TL} cross sections, which can be extracted from the Φ dependence, were, respectively, $10.6\% \pm 11.8\%$ and $0.4\% \pm 5.4\%$ of the total cross section. They are therefore consistent with zero, as they should be if SCHC is valid and, in any case, don't represent potential large violations of SCHC. Let's also note that all previous experiments on electromagnetic production of ρ^0 on the nucleon are consistent with the dominance of s -channel helicity conserving amplitudes (the helicity-flip amplitudes which have been reported [12, 13, 14, 15] never exceeded 10-20% of the helicity non-flip amplitudes). We can therefore safely rely on SCHC for our analysis.

The decay angular distribution of the π^+ in the ρ^0 rest frame can be written as [11]:

$$W(\cos\theta_{\text{hel}}) = \frac{3}{4} [1 - r_{00}^{04} + (3r_{00}^{04} - 1) \cos^2\theta_{\text{hel}}], \quad (1)$$

where r_{00}^{04} represents the degree of longitudinal polarization of the ρ meson. Under the assumption of SCHC, the ratio of longitudinal to transverse cross sections is:

$$R_\rho = \frac{\sigma_L}{\sigma_T} = \frac{1}{\epsilon} \frac{r_{00}^{04}}{1 - r_{00}^{04}}, \quad (2)$$

where ϵ is the virtual photon transverse polarization. r_{00}^{04} was extracted from the fit of the background-subtracted $\cos\theta_{\text{hel}}$ distributions following Eq. 1 as illustrated in the insert in Fig. 3, and was used in Eq. 2 to determine R_ρ .

Due to limited statistics in the CLAS data, this procedure could be performed only for the two Q^2 points which are shown on Fig. 3 and where our points are found to be compatible with the existing world's data. We then have fitted the Q^2 dependence of R_ρ including, in order to take into account a potential W dependence of the ratio R , only the world's data in the W domain close to ours ($W \approx 2.1$ GeV) [12, 16]. The following parametrization, whose power form is motivated by the perturbative PQCD prediction that σ_T is power suppressed with respect to σ_L , was found :

$$R_\rho = 0.75 \pm 0.08 \times (Q^2)^{1.09 \pm 0.14}. \quad (3)$$

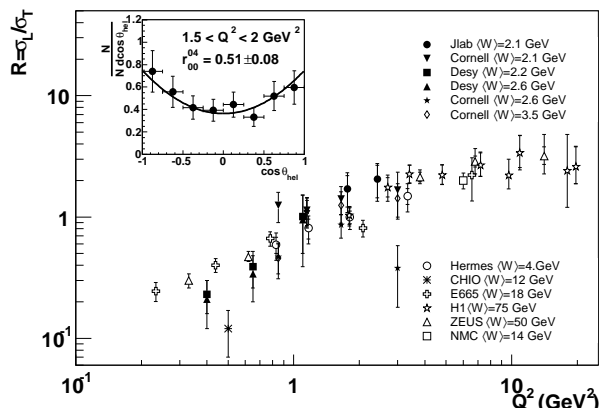


FIG. 3: The ratio $R = \sigma_L/\sigma_T$ as a function of Q^2 for ρ^0 meson electroproduction on the nucleon. The other data are from [12, 13, 14, 15, 16, 17, 18, 19, 20]. The insert shows one of our $\cos\theta_{\text{hel}}$ distributions with a fit to determine r_{00}^{04} .

It is customary to define the reduced cross section for ρ meson production as the electroproduction cross section divided by the flux of virtual photons :

$$\sigma_T + \epsilon\sigma_L = \frac{1}{\Gamma_V(Q^2, x_B)} \times \frac{d^2\sigma^{ep}}{dQ^2 dx_B}, \quad (4)$$

where the virtual photon flux is given by :

$$\Gamma_V(Q^2, x_B) = \frac{\alpha}{8\pi} \frac{Q^2}{M_p^2 E_e^2} \frac{1 - x_B}{x_B^3} \frac{1}{1 - \epsilon}. \quad (5)$$

In this notation, and in Fig. 4, the longitudinal and transverse σ_T and σ_L cross sections are integrated over t , Φ ,

θ_{hel} , and ϕ_{hel} . The t dependence of $\sigma_T + \epsilon\sigma_L$ can be parametrized by $e^{-b|t-t_{\text{min}}|}$ ($-t_{\text{min}} < -t < 1 \text{ GeV}^2$), where $-t_{\text{min}}$ is the smallest value of momentum transfer for a given kinematic bin. We measured the exponential slope b to range from 1.19 to 1.74 GeV^{-2} for x_B between 0.31 and 0.52.

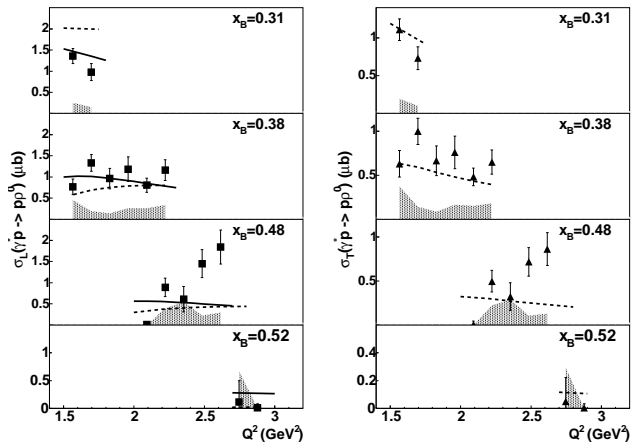


FIG. 4: Cross sections σ_L (left) and σ_T (right) for $ep \rightarrow e'p\rho^0$ as a function of Q^2 as measured in this experiment. The dotted line represents the Regge model of Refs. [21, 22] while the solid line describes the GPD model of Refs. [6, 23]. The systematic error is indicated by the shaded zones at the bottom of the plots.

The longitudinal and transverse cross sections are plotted in Fig. 4 as a function of Q^2 for four bins centered at x_B of 0.31, 0.38, 0.48, and 0.52. These values correspond to W values of 2.2, 2.0, 1.9, and 1.85 GeV, respectively. The data are compared to two theoretical approaches. The first one is based on hadronic degrees of freedom with meson Regge trajectory exchanges in the t -channel (as illustrated in Fig. 1, left graph). This approach has been successful in describing, with very few free parameters, essentially all of the available observables of a series of forward exclusive reactions in photo- and electroproduction of pseudoscalar mesons ($\pi^{0,\pm}$, K^+ [24], η , η' [25]) above the resonance region. For the ρ^0, ω, ϕ vector mesons, as well as for Compton scattering, such an approach has been recently developed in Refs. [21, 22, 26]. In the case of ρ^0 electroproduction, the contributing meson trajectories are the σ , f_2 , and Pomeron, the latter being negligible in the W region investigated in this experiment. This Regge model was normalized by adjusting the σ and f_2 meson-nucleon couplings to reproduce existing photoproduction data (see for instance, Refs. [27]). There is little freedom in the choice of parameters when one uses data from all three ρ^0, ω , and ϕ channels, which together constrain all photoproduction parameters. The only remaining free parameters for the electroproduction case are the squared mass scales of the meson monopole form factors at the electromagnetic vertices for the diagrams of Fig. 1 (left plot). They have been determined

from the Q^2 dependence of the world's data, in particular from the Cornell [16] and HERMES [28] experiments, to be approximately 0.5 GeV^2 , in accordance with known meson form factor mass scales.

As shown in Fig. 4, this Regge model provides a fair description of the transverse and longitudinal cross sections. There is some discrepancy at large values of x_B , but at those values some s -channel nucleonic resonances decaying into $\rho^0 p$ may contribute, a process which is not taken into account in this Regge t -channel approach, and might explain the missing strength in this particular kinematical domain. The calculation was also done for the Cornell [16] and HERMES [28] data, where, general agreement is found as well (the longitudinal cross section is also overestimated as one goes to smaller x_B , as in our $x_B = 0.31$ bin).

We now turn to the handbag diagram approach (Fig. 1, right plot), which is based on the QCD factorization between a “hard” process (the interaction between a quark of the nucleon and the virtual photon, along with a one-gluon exchange for the formation of the final meson) and a “soft” process (the parametrization of the partonic structure of the nucleon in terms of GPD's). As mentioned in the introduction, this approach is only valid at sufficiently large Q^2 when the longitudinal cross section dominates the QCD expansion in powers of $1/Q^2$. Unfortunately, the value of Q^2 at which the “handbag” mechanism becomes valid is unknown, and especially for meson electroproduction, it must be determined experimentally.

In the case of ρ^0 production, only the unpolarized GPD's H and E contribute to the amplitude of the reaction. In the calculation, shown in Fig. 4, we neglect the contribution due to the GPD E because it is proportional to the 4-momentum transfer between the incoming virtual photon and the outgoing meson, and our data cover small momentum transfers. For the GPD H we use the parametrization of Refs. [6, 23]. The other ingredient entering the (leading order) calculation of the handbag diagram is the treatment of the strong coupling constant α_s between the quarks and the gluon. It has been “frozen” to a value of 0.56, as determined by QCD sum rules [29]. The freezing of the strong coupling constant α_s is an effective way to average out non-perturbative effects at low Q^2 and is supported by jet-shape analysis of the infrared coupling [30].

As mentioned earlier, the handbag diagram calculation can only be compared with the longitudinal part of the cross section. Figure 4 shows a good agreement between the calculation and the data at the low x_B values. As for the Regge model discussed above, the two highest x_B bins might contain some additional nucleonic resonance “contamination”, which are not included in the “handbag” approach. Variations in reasonable ranges of the parameters entering the GPD's were studied, and results were found to be stable at the 50% level. This provides

confidence in the stability, reliability, and validity of the calculation based on the prescription of a “frozen” α_s . Let us also note that this calculation reproduces reasonably well the HERMES data [28], which were taken at neighboring kinematics.

A signature of the handbag mechanism is that, independent of any particular GPD parametrization adopted, the (reduced) cross sections should follow a $1/Q^6$ dependence at fixed t and x_B . In this analysis, due to the lack of statistics, σ_L is integrated over t , which means that it is proportional to t_{\min} , this latter variable changing as a function of Q^2 . This $1/Q^6$ scaling behavior at fixed t and x_B can therefore not be directly observed in our data, which is modified by the (trivial) kinematical Q^2 dependence of t_{\min} . Nevertheless, agreement between the data and the GPD calculation, which also contains this trivial t_{\min} dependence, should be interpreted as confirmation of the leading order prediction based on the “handbag” diagram.

In conclusion, we have presented here a first exploration of exclusive vector meson electroproduction on the nucleon in a region of Q^2 between 1.5 and 3.0 GeV² and x_B between 0.2 and 0.6, which is a kinematical domain barely explored. The Regge model, based on “economical” hadronic degrees of freedom, is able to describe the transverse cross section data, along with the other existing vector meson photo- and electroproduction data. Furthermore, the more fundamental “handbag” approach, with a standard parametrization of the GPD H and the extrapolation to low Q^2 by an effective freezing of α_s , provides a fair description of the longitudinal part of the cross section. Therefore it seems possible to understand the longitudinal part of the ρ meson production cross section in a pQCD framework, which potentially gives access to GPD’s. The transverse cross section, on the other hand, for which no factorization between soft and hard physics exists, can be described in terms of meson exchanges. These tentative conclusions need of course to be confirmed by a more extensive and thorough exploration of the x_B, Q^2 phase space which is currently under way with a much larger data set [31].

We would like to acknowledge the outstanding efforts of the staff of the Accelerator and the Physics Divisions at Jefferson Lab that made this experiment possible. This work was supported in part by the Istituto Nazionale di Fisica Nucleare, the French Centre National de la Recherche Scientifique, the French Commissariat à l’Energie Atomique, the U.S. Department of Energy, the National Science Foundation, Emmy Noether grant from the Deutsche Forschungsgemeinschaft and the Ko-

rean Science and Engineering Foundation. The South-eastern Universities Research Association (SURA) operates the Thomas Jefferson National Accelerator Facility for the United States Department of Energy under contract DE-AC05-84ER40150.

-
- [1] J.C. Collins, L. Frankfurt and M. Strikman, Phys. Rev. D **56** (1997) 2982.
 - [2] L. Frankfurt, W. Koepf and M. Strikman, Phys. Rev. D **54** (1996) 3194
 - [3] X. Ji, Phys. Rev. Lett. **78** (1997) 610; Phys. Rev. D **55** (1997) 7114.
 - [4] A.V. Radyushkin, Phys. Lett. B **380** (1996) 417; Phys. Rev. D **56** (1997) 5524.
 - [5] D. Müller, D. Robaschik, B. Geyer, F.-M. Dittes, and J. Horejsi, Fortschr. Phys. **42** (1994) 101.
 - [6] M. Vanderhaegen, P.A.M. Guichon and M. Guidal, Phys. Rev. Lett. **80** (1998) 5064; Phys. Rev. D **60** (1999) 094017.
 - [7] B. Mecking *et al.*, Nucl. Inst. Meth. A **503** (2003) 513.
 - [8] P. Corvisiero *et al.*, Nucl. Inst. Meth. A **346** (1994) 433.
 - [9] L.W. Mo, Y.S. Tsai, Rev. Mod. Phys. **41** (1969) 205.
 - [10] T.H. Bauer *et al.*, Rev. of Mod. Phys. **50**, No.2, (1978) 261.
 - [11] K. Schilling and G. Wolf, Nucl. Phys. B **61** (1973) 381.
 - [12] P. Joos *et al.*, Nucl. Phys. B **113** (1976) 53.
 - [13] C. Adloff *et al.*, Eur. Phys. J. C **13** (2000) 371; S. Aid *et al.*, Nucl. Phys. B **468** (1996) 3.
 - [14] J. Breitweg *et al.*, Eur. Phys. J. C **12** (2000) 393.
 - [15] A.B. Borissov *et al.*, HERMES Report 01-060 (2001).
 - [16] D.G. Cassel *et al.*, Phys. Rev. D **24** (1981) 2787.
 - [17] M. Tytgat, PhD thesis, HERMES Report 01-014 (2001)
 - [18] M.R. Adams *et al.*, Z. Phys. C **74** (1997) 237.
 - [19] W.D. Shambroom *et al.*, Phys. Rev. D **26** (1982) 1.
 - [20] N. Arneado *et al.*, Nucl. Phys. B **429** (1994) 503.
 - [21] F. Cano and J.-M. Laget, Phys. Lett. B **551** (2003) 317.
 - [22] J.-M. Laget, Phys. Lett. B **489** (2000) 313.
 - [23] K. Goeke, M.V. Polyakov and M. Vanderhaegen, Prog. Part. Nucl. Phys. **47** (2001) 401.
 - [24] M. Guidal, J.-M. Laget and M. Vanderhaeghen, Phys. Lett. B **400** (1997) 6; Nucl. Phys. A **627** (1997) 645; Phys. Rev. C **57** (1998) 1454; Phys. Rev. C **61** (2000) 025204; Phys. Rev. C **68** (2003) 058201.
 - [25] W.-T. Chiang, S. N. Yang, L. Tiator, M. Vanderhaeghen, D. Drechsel, Phys. Rev. C **68** (2003) 045202.
 - [26] J.-M. Laget, Nucl. Phys. A **699** (2002) 184.
 - [27] M. Battaglieri *et al.*, Phys. Rev. Lett. **87** (2001) 172002; Phys. Rev. Lett. **90** (2003) 022002.
 - [28] A. Airapetian *et al.*, Eur. Phys. J. C **17** (2000) 389.
 - [29] P. Ball and V.M. Braun, Phys. Rev. D **54** (1996) 2182.
 - [30] Y. Dokshitzer, Phil. Trans. Roy. Soc. Lond. A **359** (2001) 309, hep-ph/0106348.
 - [31] JLab experiment E99-105, spokesperons M. Garçon, M. Guidal and E. Smith.